ELECTRONIC SUPPLEMENTARY INFORMATION

Self-assembly behavior of experimentally realizable lobed patchy particles

Sanjib Paul and Harish Vashisth*

Department of Chemical Engineering, University of New Hampshire, 33 Academic Way, Durham, NH 03824, USA

* Corresponding author; Email: harish.vashisth@unh.edu

MODELS AND METHODS

A. Interaction Potential

All three types of interactions (lobe-lobe, seed-seed, and seed-lobe) are modeled by a surface shifted Lennard-Jones potential. The functional form of the SSLJ potential acting between the particle i and the particle j is

$$V_{\mathrm{SSLJ}}(r) = 4\epsilon_{ij}\left[\left(\frac{\sigma}{r-\Delta}\right)^{12} - \left(\frac{\sigma}{r-\Delta}\right)^{6}\right], \tag{S1}$$

where ϵ_{ij} is the energy well depth for the i-j pair and $\Delta = (\sigma_i + \sigma_j)/2 - \sigma$, where σ_i and σ_j are the diameters of the particle i and j, respectively.

B. Simulation Details

The ϵ_{LL}, ϵ_{SS}, and ϵ_{LS} (L and S stand for lobes and seeds, respectively) are equal to 1 in each case. The value of σ is equal to 1.0 for all three types of interactions. Cut-off distances, r_{cut}, for seed-seed pairs and for seed-lobe pairs were set to $2^{1/6}$ σ_L to make these interactions repulsive, and for lobe-lobe pairs it was set to 3.0 σ_L to make these interactions attractive. For each particle, the bonds between the lobes and the seed, and the angles between the lobes with respect to the seed are modeled by harmonic potentials. The force constants for the bonds and angles are adjusted in a way that lobes are stable around the seed. For each type of lobed particle, we carried out 36 simulations (at 6 different seed diameters and at 6 different temperatures). Therefore, a total of 180 simulations were performed for all five types of particles. Each simulation was carried out in a cubic simulation domain with a side length of 100 σ_L for a total of 10^8 steps and using a time step of 0.005. Each simulation domain contained 8000 lobed particles of each type. The number density (ρ_N) of particles in each simulation domain is 0.008. We also carried out 9 additional simulations for each type of particle at three higher number densities (ρ_N = 0.016, 0.037, 0.125) and at three selected combinations of seed diameters and temperatures. In these simulations, we reduced the dimensions of simulation domains (80 σ_L, 60 σ_L, and 40 σ_L) keeping the number of particles fixed.

C. Metrics for Assessing Self-assembled Structures

We calculated the radial distribution function (RDF) between the pair of seeds to distinguish between different self-assembled structures generated at different seed diameters and temperatures. The RDF is defined by the equation

$$g_{\mathrm{SS}}(\mathrm{r}) = \frac{\rho(\mathrm{r})}{\rho_o}, \tag{S2}$$

where ρ(r) is the number density of particles at a distance r from a reference particle and ρ_o is the bulk density. The characteristics of RDFs are different for different self-assembled structures, as described below.

(i) *Random aggregates*: There is no order between the seeds, even at very short distances. These aggregates do not possess any specific shape.

(ii) *Spherical aggregates*: These type of aggregates are spherical in shape, and the seeds in these aggregates are randomly arranged. The only difference between the random and spherical aggregates is that the random aggregates can appear in different shapes (cylindrical, wire like) and the spherical aggregates appear only in a spherical shape.

(iii) *Liquid droplets*: These types of self-assembled structures form well-defined second and third coordination shells. Therefore, we observe one or two broad peaks (apart from the first intense peak corresponding to the first coordination shell) in the RDFs.

(iv) *Crystalline structures*: In these structures, seeds are well ordered. We observed several intense peaks in the RDFs at a regular interval for a given crystalline structure.

FIGURES

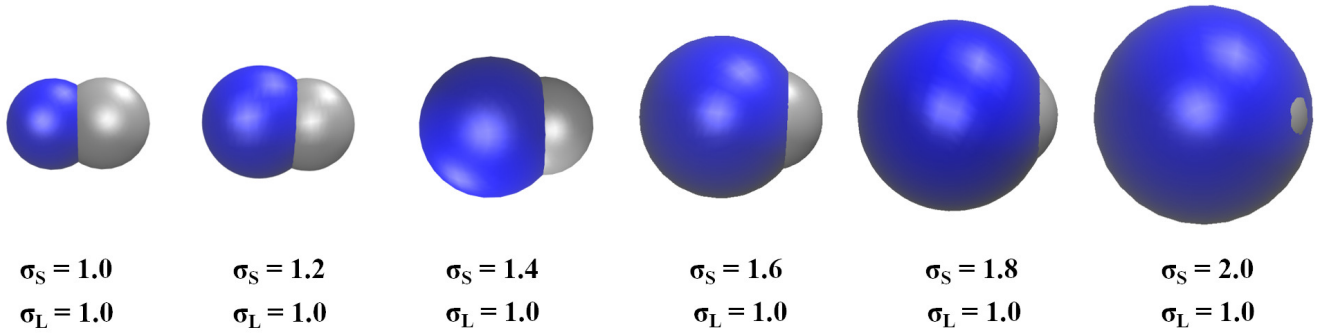

FIG. S1 Modeling of snowman shaped particles. The seed (blue) and lobe (gray) are kept at a 0.5 σ_L apart. The diameter of the seed is gradually increased from $\sigma_S = 1.0$ to 2.0 to control the lobe size.

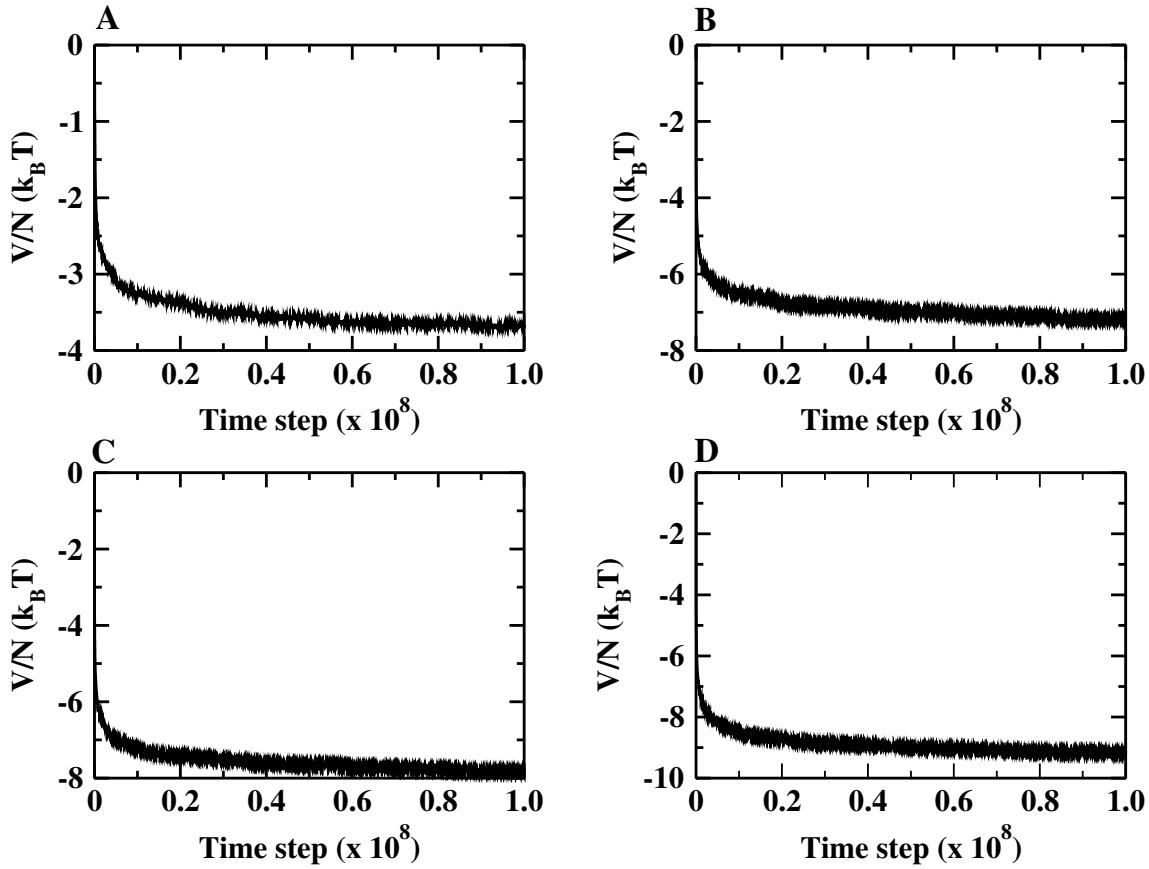

FIG. S2 Four representative plots showing the change in potential energy per particle (V/N) with time for (A) dumbbell, (B) trigonal planar, (C) square planar, and (D) tetrahedral lobed particles at $\sigma_S = 1.4$ and $k_BT = 0.4$. Toward the end of each simulation, there is no significant change in the potential energy, indicating that the systems arrive at equilibrium and the self-assembled structures are equilibrium structures. We observed similar trends in the potential energy for other systems.

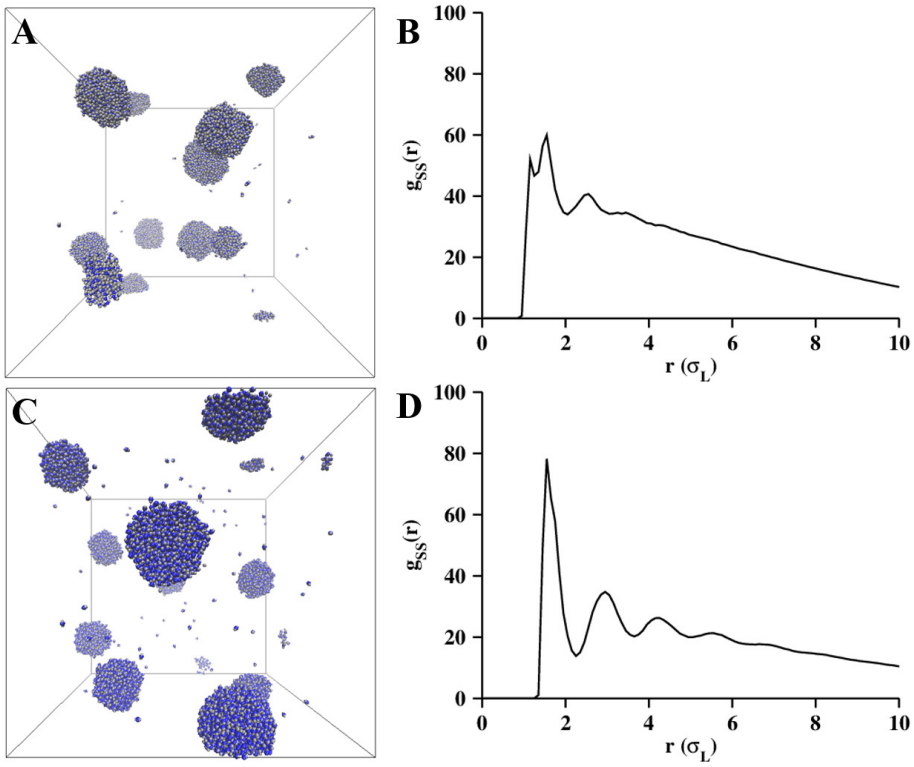

FIG. S3 Self-assembly of dumbbell shaped particles at higher temperatures. Simulation domain showing (A) spherical random aggregates at $\sigma_S = 1.0$ and $k_BT = 0.6$ and (C) spherical liquid like droplets at $\sigma_S = 1.4$ and $k_BT = 0.4$. The corresponding RDFs are also shown in panels B and D.

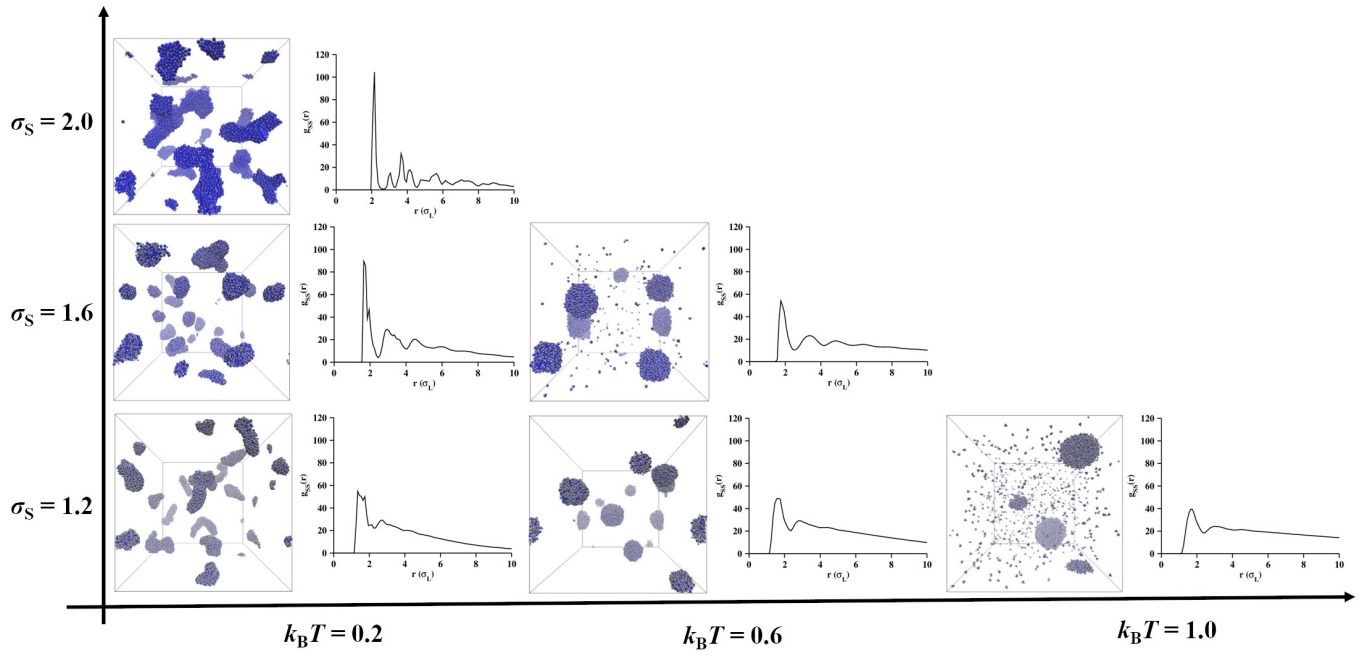

FIG. S4 Morphologies and corresponding RDFs are shown for trigonal planar particles at various σ_S and k_BT.

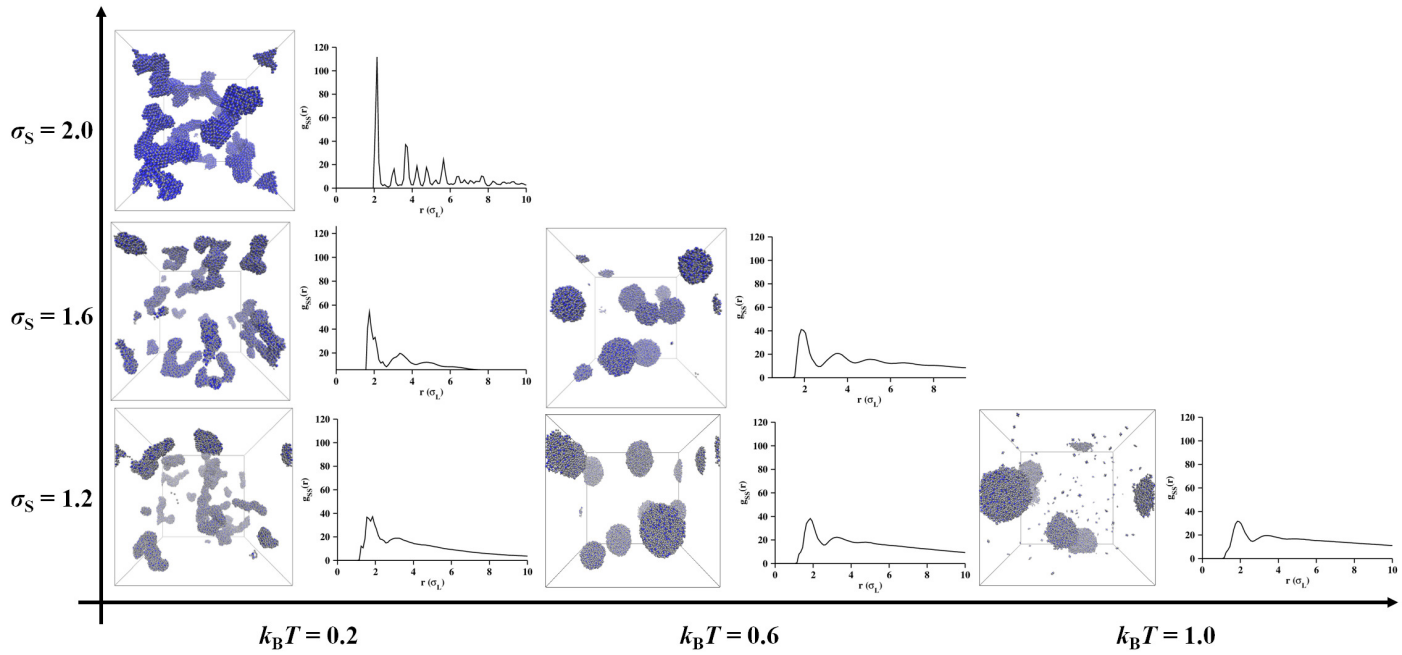

FIG. S5 Data similar to Fig. S4 are shown for square planar particles.

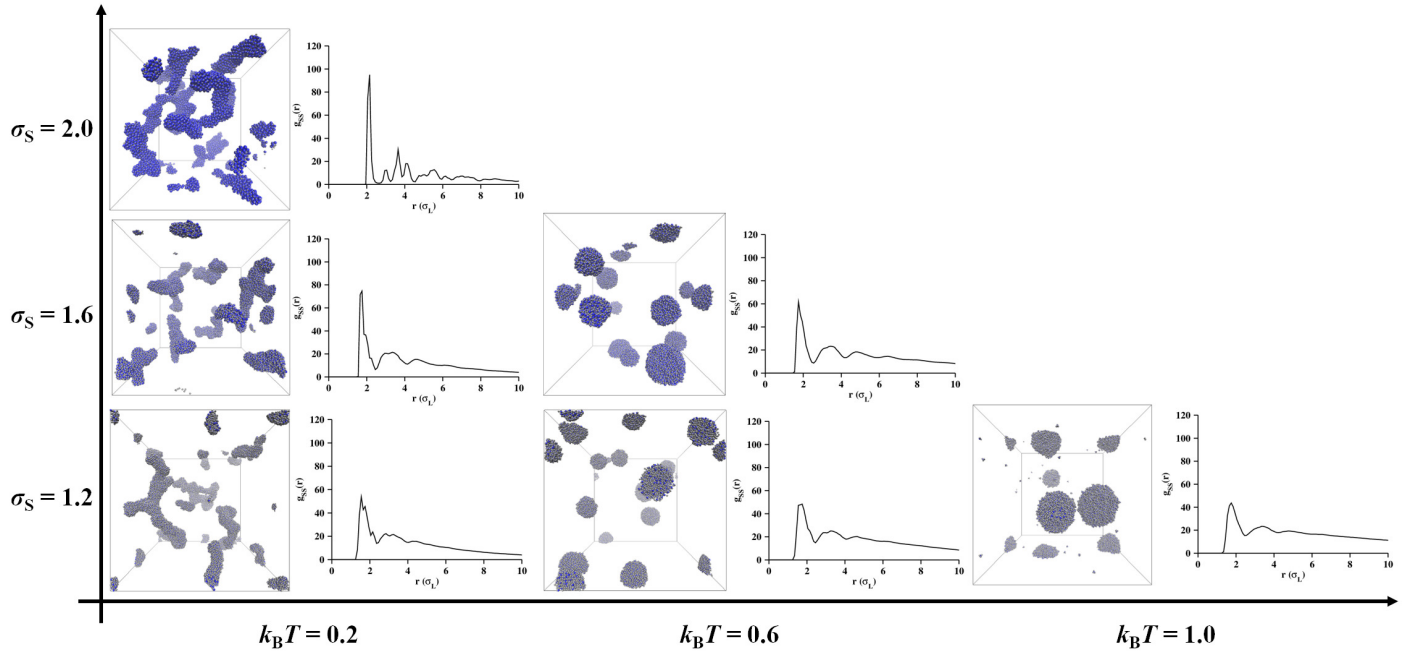

FIG. S6 Data similar to Fig. S4 are shown for tetrahedral lobed particles.

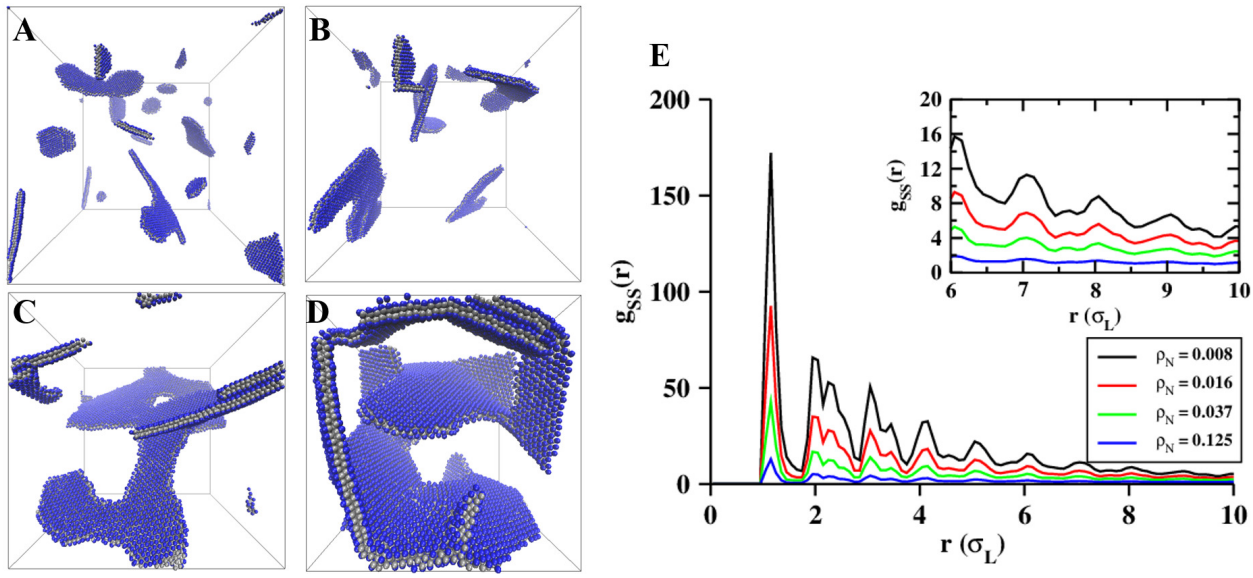

FIG. S7 Self-assembled structures (two-dimensional sheets) generated by snowman shaped particles at $\sigma_S = 1.0$ and $k_BT = 0.2$ at four different number densities of particles: $\rho_N = 0.008$ (A), 0.016 (B), 0.037 (C), and 0.125 (D). As we increase ρ_N, the size of two-dimensional sheets increases. The radial distribution functions are shown in panel E. The height of each peak decreases with an increase in ρ_N. At $\rho_N = 0.125$, $g_{SS}(r)$ is converged to 1 at longer distances (the blue curve in the inset).

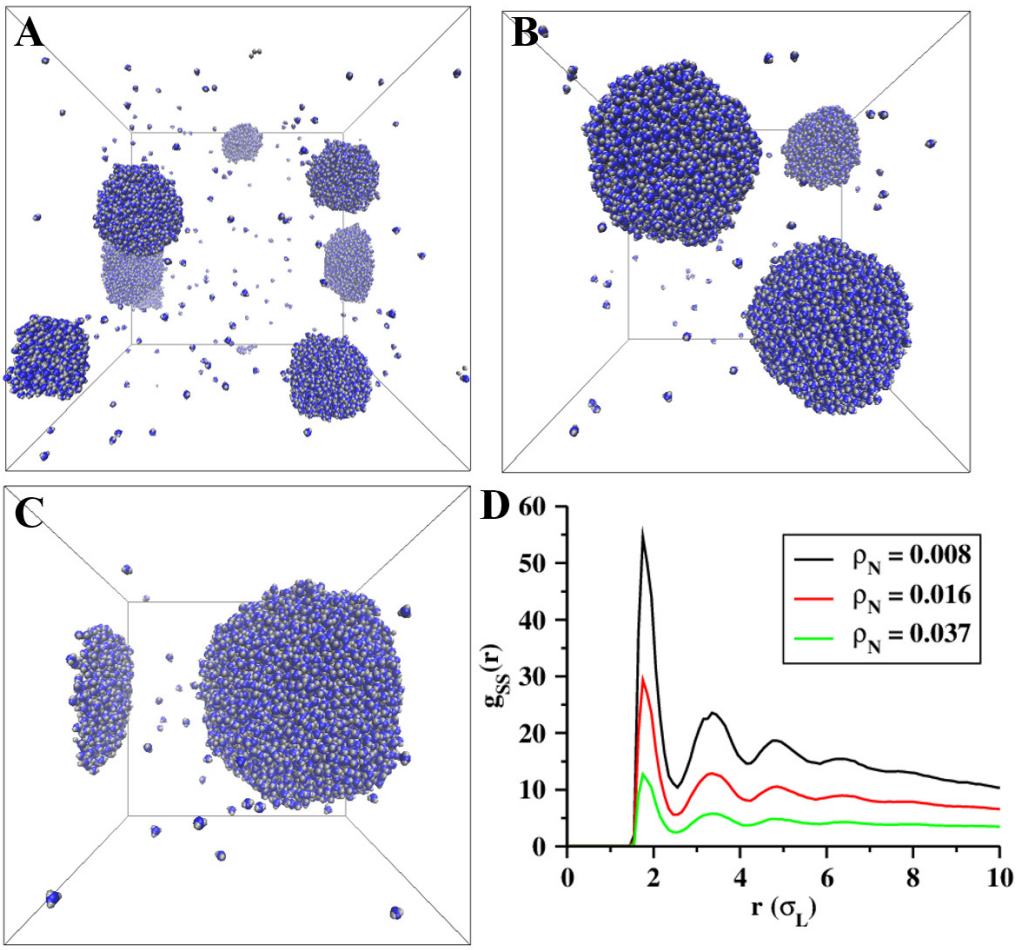

FIG. S8 Self-assembled structures (liquid droplets) generated by trigonal planar shaped particles at $\sigma_S = 1.6$ and $k_BT = 0.6$ at three different number densities of particles: $\rho_N = 0.008$ (A), 0.016 (B), and 0.037 (C). As we increase ρ_N, the size of each liquid droplet increases. The radial distribution functions for self-assembled structures are shown in panel D.

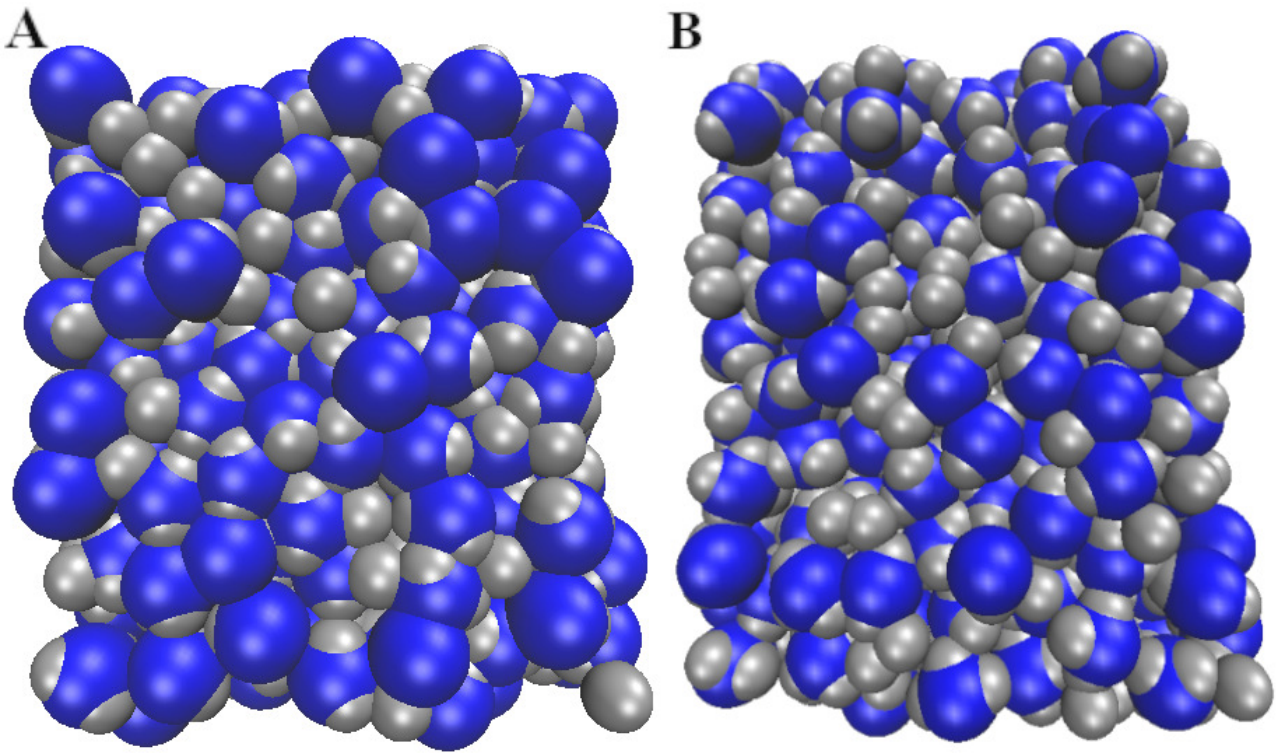

FIG. S9 Two representative cubes extracted for calculating pore size distributions: (A) trigonal planar particles and (B) square planar particles.

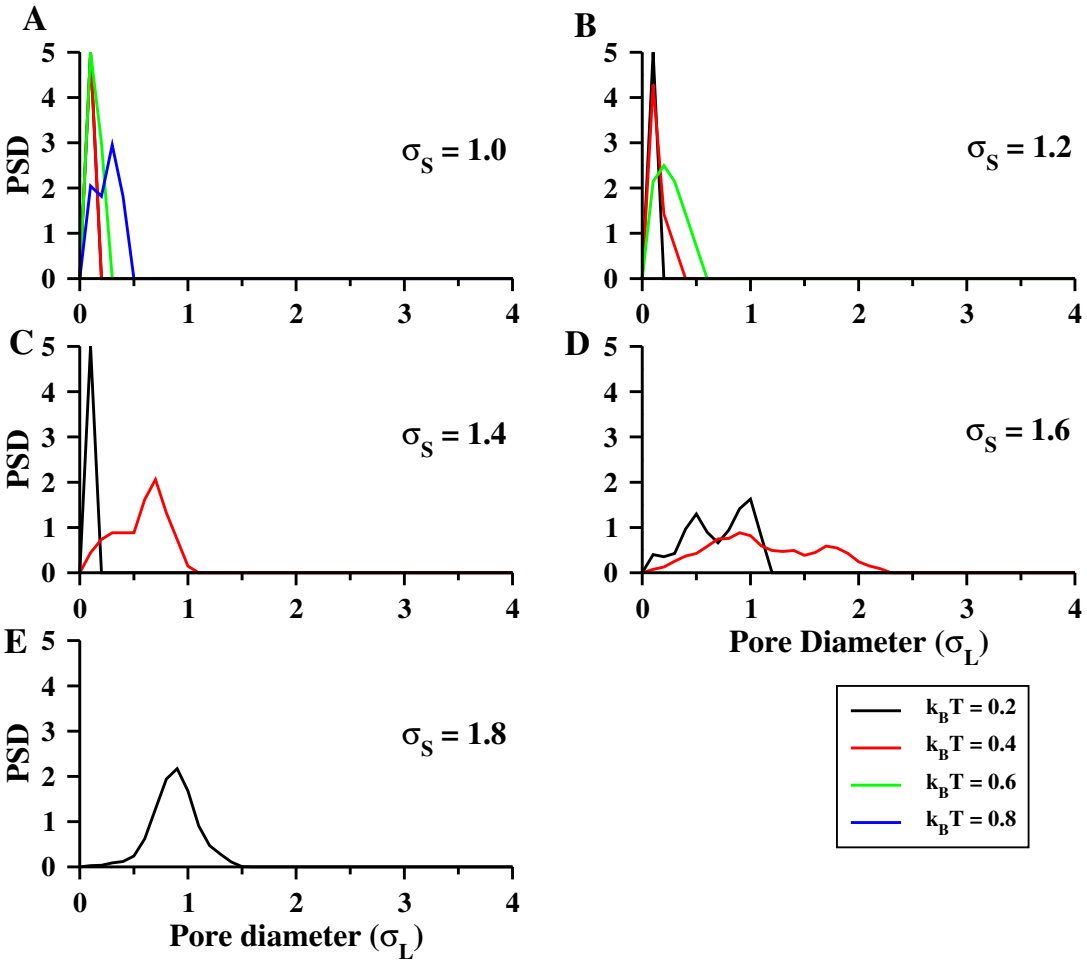

FIG. S10 Pore size distributions for dumbbell particles at different seed diameters. Color indicates distributions corresponding to different k_BT.

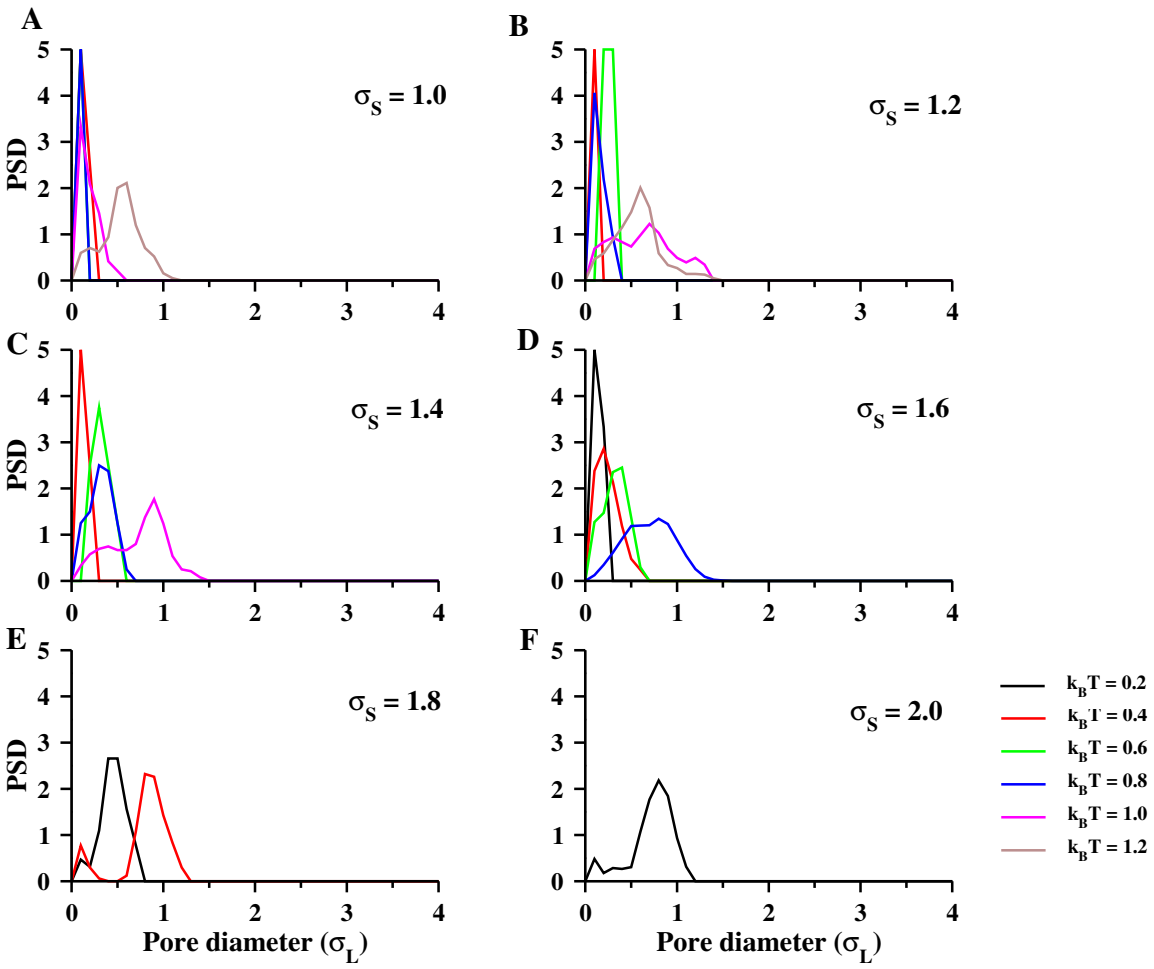

FIG. S11 Data similar to Fig. S10 are shown for trigonal planar particles.

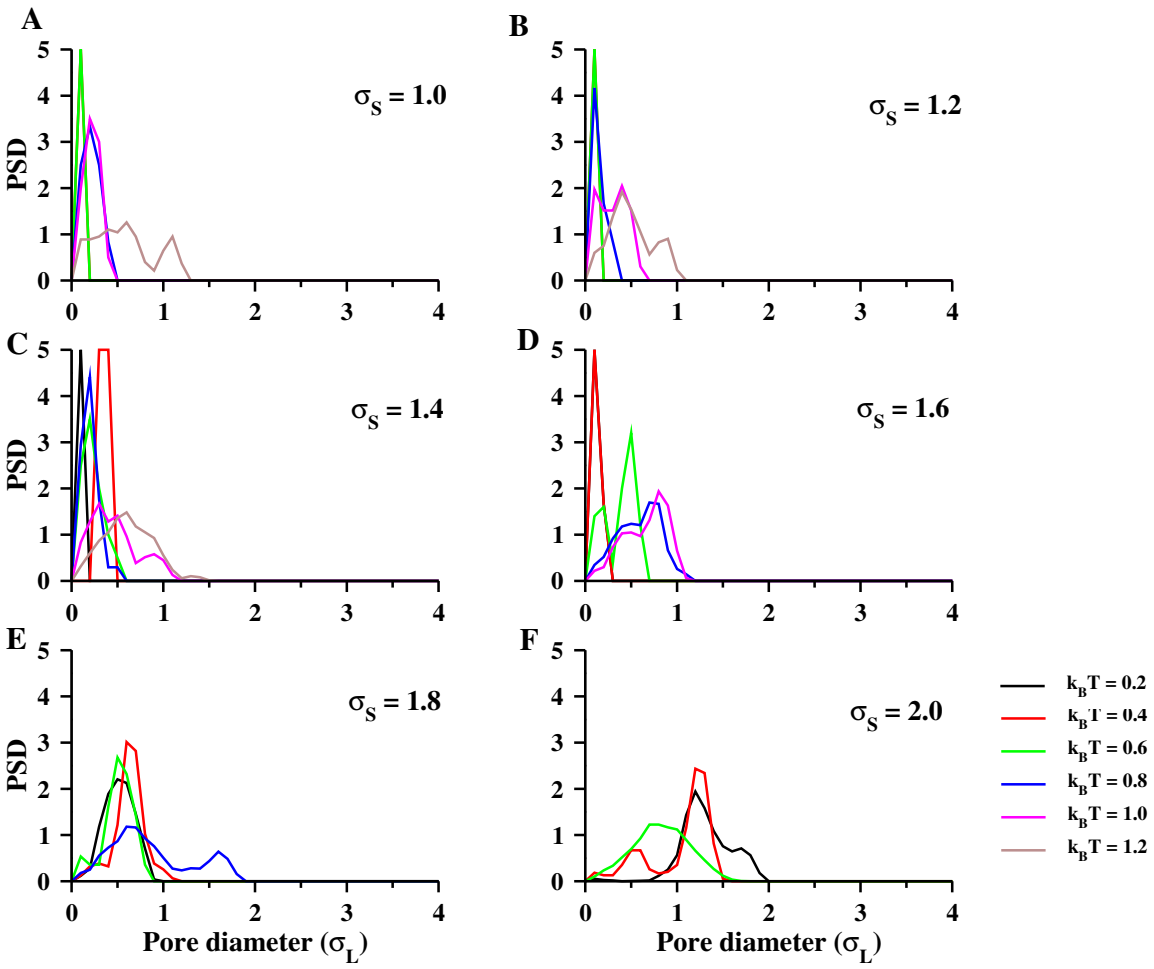

FIG. S12 Data similar to Fig. S10 are shown for square planar particles.

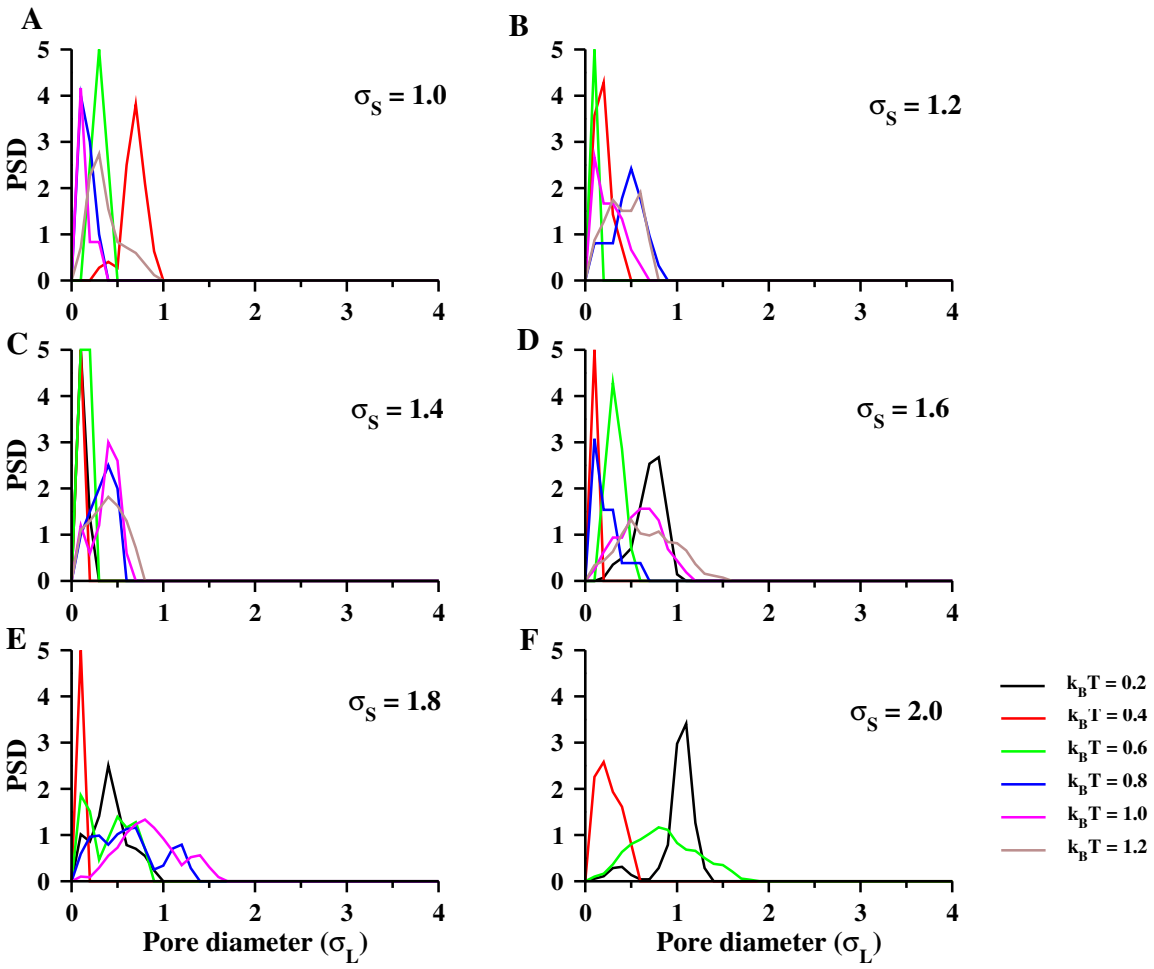

FIG. S13 Data similar to Fig. S10 are shown for tetrahedral particles.